

# Momentum Memory for Knowledge Distillation in Computational Pathology

Yongxin Guo<sup>1\*</sup> Hao Lu<sup>1</sup> Onur C. Koyun<sup>1</sup>  
Zhengjie Zhu<sup>1</sup> Muhammet Fatih Demir<sup>1</sup> Metin Nafi Gurcan<sup>1</sup>

<sup>1</sup>Wake Forest University School of Medicine, Winston-Salem, NC, USA

{Hao.Lu, Onur.Koyun, muhammet.demir}@advocatehealth.org

{Yongxin.Guo, Zhengjie.Zhu, Metin.Gurcan}@wfusm.edu

## Abstract

Multimodal learning that integrates genomics and histopathology has shown strong potential in cancer diagnosis, yet its clinical translation is hindered by the limited availability of paired histology–genomics data. Knowledge distillation (KD) offers a practical solution by transferring genomic supervision into histopathology models, enabling accurate inference using histology alone. However, existing KD methods rely on batch-local alignment, which introduces instability due to limited within-batch comparisons and ultimately degrades performance. To address these limitations, we propose Momentum Memory Knowledge Distillation (MoMKD), a cross-modal distillation framework driven by a momentum-updated memory. This memory aggregates genomic and histopathology information across batches, effectively enlarging the supervisory context available to each mini-batch. Furthermore, we decouple the gradients of the genomics and histology branches, preventing genomic signals from dominating histology feature learning during training and eliminating the modality-gap issue at inference time. Extensive experiments on the TCGA-BRCA benchmark (HER2, PR, and ODX classification tasks) and an independent in-house testing dataset demonstrate that MoMKD consistently outperforms state-of-the-art MIL and multimodal KD baselines, delivering strong performance and generalization under histology-only inference. Overall, MoMKD establishes a robust and generalizable knowledge distillation paradigm for computational pathology.

## 1. Introduction

Deep multiple instance learning (MIL) models trained solely on histopathology slides have achieved strong performance [13, 14, 25, 29, 41], yet their predictive ceiling

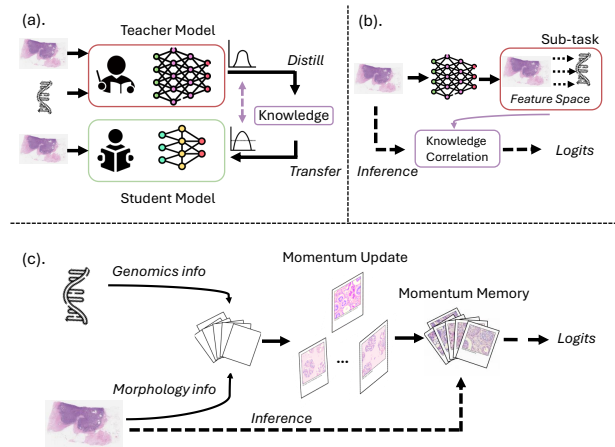


Figure 1. a. the classical teacher-student knowledge distillation (KD) method. b. the correlation-based KD method. c. the proposed momentum memory KD method. Compared with a and b, the proposed method uses momentum memory for knowledge distillation to solve the batch-local problem.

remains constrained by the limited information in the image representation. Many clinically important biomarkers, for example, molecular subtypes, gene-expression signatures, or recurrence risk scores, are defined not by visual appearance but by underlying molecular signals [36]. High-throughput transcriptomic assays can capture this information directly [3, 24]. Multimodal learning that integrates genomics with histopathology has shown improved performance by combining these complementary sources of information [8, 9, 35]. However, genomic data are expensive and slow, especially in resource-limited settings. To circumvent this limitation, recent studies have explored knowledge distillation (KD) to inject genomic information into histology models during training, enabling histology-only inference while retaining molecular predictive power.

Existing KD frameworks transfer supervision from a multimodal teacher (e.g., histology with omics) to a uni-

\*Corresponding author: Yongxin.Guo@wfusm.edu

modal student (histology-only) [7, 17, 23, 34]. However, most existing frameworks in pathology domain operationalize KD as *batch-local, continuous feature matching*: either forcing heterogeneous modalities map into the same latent space [19, 23, 34] (Fig. 1a) or regressing auxiliary cross-modal targets and treating them as distilled knowledge [31, 42] (Fig. 1b). Such intra-batch supervision is inherently fragile. Its supervision signal is transient, which defined only by the current mini-batch, and offers limited negative sample diversity. This forces an unstable, direct alignment between asymmetric modalities (e.g., genomics data and pathology image). This fragility is further amplified in the pathological MIL setting. The information redundancy of gigapixel images, where noisy background regions dominate the mini-batch, simply overwhelms the distillation signal, leading to brittle generalization under domain shift.

We address these limitations by reframing cross-modal KD into a memory-based alignment framework, where features are matched to a large and consistent momentum memory instead of relying on unstable batch-level regression. We propose Momentum Memory for Knowledge Distillation (MoMKD), which maintains a slowly evolving, label-conditioned momentum memory. Similarly to dynamic dictionaries in contrastive learning [16], the memory aggregates genomics-histopathology information across the entire training trajectory. It simultaneously serves as an information bottleneck that compresses redundant histology features and as an distillation mediator that injects genomic semantics into histology representations (Fig. 1c). MoMKD operates through two key mechanisms. First, a soft angle-based memory aligns both modalities to the shared memory space, enlarging the supervisory context across each mini-batch. Second, a gradient-decoupled update strategy isolates the genomic and histology branches, preventing genomic gradients from overwhelming histology features during training and eliminating the modality gap in the uni-modal inference stage.

We validate MoMKD across three classification tasks (HER2, PR, and Oncotype DX) on the TCGA-BRCA benchmark and an independent institutional cohort. MoMKD consistently outperforms state-of-the-art MIL and multimodal KD baselines, demonstrating superior cross-domain generalization. Overall, MoMKD introduces a new cross-modal distillation paradigm that replaces high-variance batch-level alignment with a stable, compact momentum memory, enabling robust multimodal knowledge distillation.

In summary, our contributions are threefold:

1. **Momentum memory for cross-modal distillation:** A label-conditioned, dynamically evolving dictionary that accumulates genomics-histopathology statistics, replacing stochastic batch-local matching with stable

dictionary-based alignment.

2. **Gradient-decoupled optimization:** A decoupling strategy that isolates genomics and histology gradients, preventing modality-gap issues between multimodal training and unimodal inference.
3. **Extensive validation and analysis:** Demonstrating strong performance and generalization across datasets, with visualizations showing that the learned memory captures meaningful biological structures.

## 2. Related Works

### 2.1. Application of MIL in WSIs

Multiple Instance Learning (MIL) is the prevailing paradigm in computational pathology: a WSI is treated as a bag of instances with slide-level supervision, enabling weakly supervised prediction. Early and influential methods like ABMIL [18] introduced attention mechanisms to learn the importance of each instance for the slide-level prediction. Subsequent work such as CLAM [22], improving the attention mechanism for better interpretability, and transformer-based architectures leveraging self-attention to model long-range dependencies between patches [4, 27].

To better capture the tumor microenvironment, recent approaches have shifted towards graph-based MIL [2, 21]. This has led to improved performance on tasks that rely on contextual information. However, a fundamental limitation persists across all WSI-only frameworks: their performance is bounded by the morphological information present in the H&E stain. For tasks inherently defined by molecular state (e.g., gene expression-based risk scores), the visual signal is often insufficient, creating a performance ceiling that motivates integrating privileged molecular data.

### 2.2. Multi-modal Knowledge Distillation for WSI analysis

To break the performance ceiling of WSI-only models, the Knowledge Distillation (KD) which leverages paired histogenomic data during training while keeps inference WSI-only has emerged as a pragmatic solution [12, 40]. In the domain of pathology image analysis, teacher-student method is one of the most popular streams [5, 28, 30]. For example, Xing et al. [34] proposed a gradient-based teacher-student framework for the tumor grading task. Compared with this two-stage KD method, Zhang et al. [38] proposed an online learning paradigm based on a multi-teacher framework for biomarker prediction. Additionally, G-HANet [31] reconstructed functional genomic information from WSI via the cross-modal learning and conducted distillation for survival analysis.

Despite progress, batch-local feature regression limits cross-modal KD: supervision hinges on mini-batch idiosyncrasies, limited-class samples are confined in-batch,

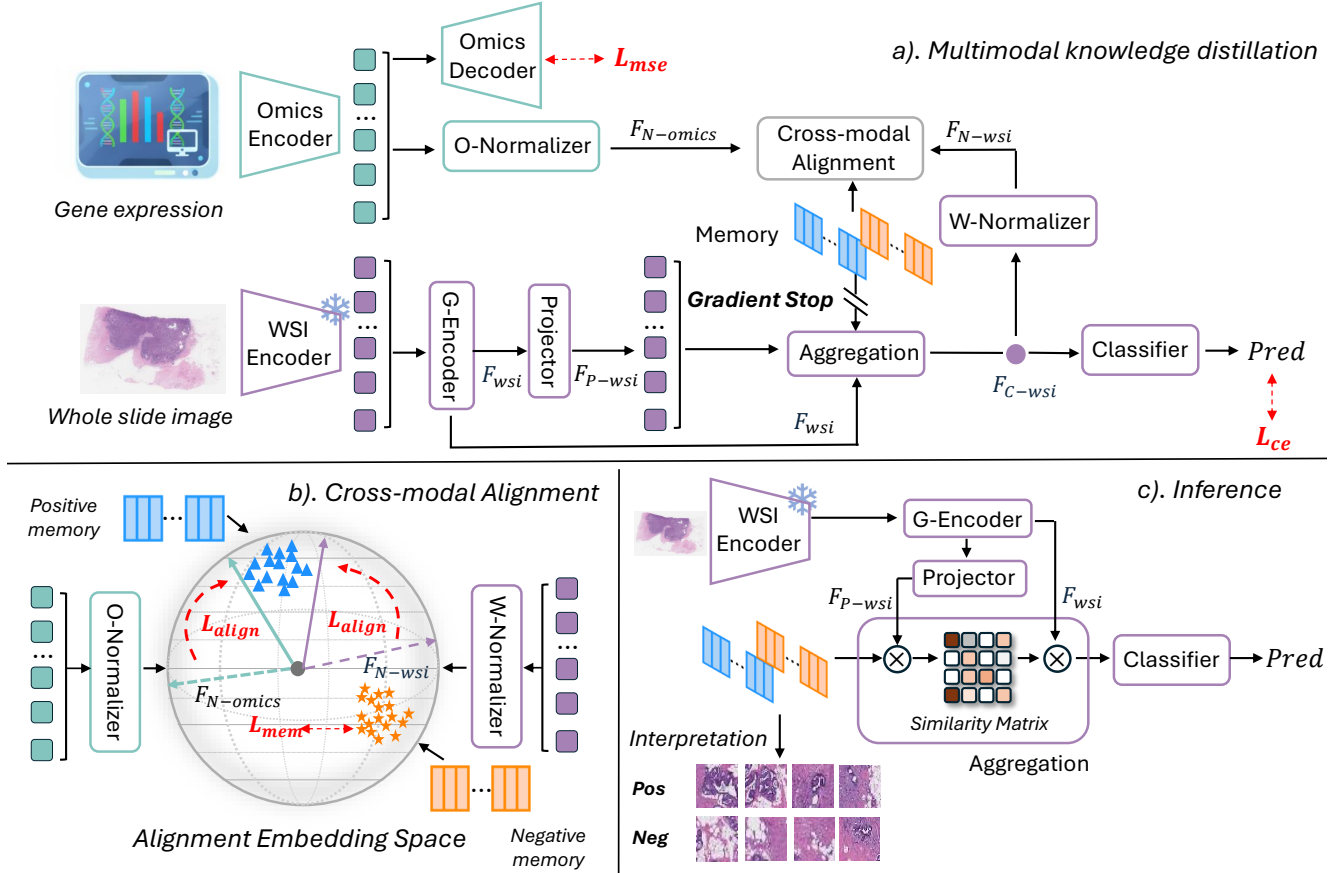


Figure 2. The overall framework of the proposed momentum memory knowledge distillation framework. a) presents the multi-modal KD training process; b) indicates the proposed cross-modal alignment. Here we assume the input is a positive case so that the alignment loss is aiming to push it closer to the positive memory set (blue triangle) and pull it away to the negative memory set (yellow star); c) presents the uni-modal inference stage, and the visual interpretation on the memory.

and heterogeneous geometries are forced to match, which yields brittle generalization under shift. This exact challenge was a critical hurdle in self-supervised representation learning. The field’s evolution provides a clear blueprint: SimCLR demonstrated the need for massive batches [10], while memory banks [33] and dynamic dictionaries, such as MoCo [16] and lots of variations [15, 39] showed that a large and consistent dictionary is the key to stable learning and robust transferability. Inspired by this, we introduce MoMKD, which adapts the momentum dictionary look-up concept to the cross-modal KD challenge. The momentum memory acts as a dynamic, global dictionary, accumulating genomics-histopathology statistics over the entire training trajectory which allows MoMKD to align modalities via a stable, shared semantic space, rather than through direct and noisy feature matching.

### 3. Methodology

#### 3.1. Overview

Computational pathology faces an intrinsic asymmetry in cross-modal distillation: global transcriptomic embeddings versus local histopathology representations. Direct and batch-local feature alignment magnifies modality noise and leads to unstable optimization.

To overcome this, we reformulate cross-modal alignment by learning a momentum memory as the distillation mediator rather than forcing direct feature matching. Specifically, both modalities interact through a compact and information-rich memory which capturing canonical genomics-histopathology joint concepts (Figure 2). In the following section, we will introduce more details of the proposed method.

#### 3.2. Dual-Branch Encoding

To model the tumor microenvironment, MoMKD employs a dual-branch encoder comprising a graph-based WSI en-

coder and a fully connected omics encoder. Both modalities are projected into a shared,  $L_2$ -normalized latent space for cross-modal alignment while preserving modality-specific structure.

**Graph-based WSI encoder.** Each WSI  $x_i$  is represented as a spatial graph  $G = (V, E)$ , where nodes  $V = \{v_1, \dots, v_I\}$  correspond to image patches and edges  $E$  connect each node to its  $k$ -nearest neighbors ( $k=8$ ) based on centroid distance. A two-layer GATv2 [6] encodes contextualized patch embeddings  $F_{\text{wsi}} = f_{\text{wsi}}(x_i) \in \mathbb{R}^{I \times D}$  ( $D=256$ ). The projected features  $F_{\text{p-wsi}} = W_{\text{proj}} \cdot F_{\text{wsi}} \in \mathbb{R}^{I \times D}$  are compared with the memory  $\mathcal{C}$  to produce similarity scores. Aggregating these patch-level similarities yields a slide-level representation  $F_{\text{C-wsi}}$ . For the cross-modal alignment,  $F_{\text{C-wsi}}$  will be linearly transformed and projected onto a spherical space as the WSI representation:

$$\mathbf{F}_{\text{N-wsi}} = \frac{W_{\text{C-wsi}} \cdot \mathbf{F}_{\text{C-wsi}}}{\|W_{\text{C-wsi}} \cdot \mathbf{F}_{\text{C-wsi}}\|_2} \in \mathbb{R}^{D_N} \quad (1)$$

where  $W_{\text{C-wsi}}$  denotes learnable weights,  $D_N=128$ .

**Omics encoder.** A lightweight MLP first projects the omics vector into the same latent space:

$$F_{\text{omics}} = f_{\text{omics}}(\text{omics}) \in \mathbb{R}^D \quad (2)$$

The resulting embedding is then transformed and  $L_2$ -normalized:

$$\mathbf{F}_{\text{N-omics}} = \frac{W_{\text{omics}} \cdot \mathbf{F}_{\text{omics}}}{\|W_{\text{omics}} \cdot \mathbf{F}_{\text{omics}}\|_2} \in \mathbb{R}^{D_N} \quad (3)$$

### 3.3. Momentum Knowledge-distillation via Cross-Modal Alignment

#### 3.3.1. Momentum Memory as Knowledge Mediator

A fundamental challenge in multi-modal learning is the modality gap. To solve this problem, we introduced a momentum memory. This compact set of class-conditional memory setting:  $C^+$  and  $C^-$  represent positive class and negative class with  $n$  memory components ( $c_j^+$  and  $c_j^-$ ,  $j = [1, \dots, n]$ ) serve as the distillation mediator and anchor both modalities to a common decision geometry. Within the training progress, more information from both omics and WSI will be compressed and accumulated to this memory, which represents the global semantic representation rather than a simple instance cache. Consequently, the model aligns heterogeneous features with this highly-compressed, slowly-evolving mediator, rather than chasing a noisy, rapidly-updating intra-batch distribution.

#### 3.3.2. Indirect Memory-based Distillation

Our distillation is an indirect process: omics and WSI features do not teach each other directly. Instead, both modalities are forced to align with the shared momentum memory. The overall workflow can be explained as below:

Before training, we let the memory have a quick look at the image data: we randomly collect 10000 patches and perform K-means clustering for the initialization. By doing this, the starting epoch can be more stable and meaningful.

**Semantic Anchoring via Omics Alignment.** This step injects the visually initialized memory with genomics-grounded semantics. Before this injection can occur effectively, we must ensure that the omics representation itself is biologically faithful and robust to noise. We achieve this by constraining the omics encoder with a self-supervised reconstruction task, which forces the omics embedding preserving the salient genetic signals during the alignment. With a robust omics embedding thus guaranteed, the omics projection  $F_{\text{N-omics}}$  is pushed to align with its corresponding memory (e.g.,  $C^+$ ) and rather than the other ( $C^-$ ). This process anchors memory to well-defined genomics concepts. For instance,  $C^+$  transitions from being merely a cluster of visual patterns to representing a stable archetype of the omics-defined pattern. This two-fold omics alignment objective, maintaining biological stability through reconstruction while learning separability, ensures the memory is accurate and discriminative.

**Knowledge Transfer via WSI Alignment.** Simultaneously, the aggregated WSI projection,  $F_{\text{N-wsi}}$ , is forced to align with the omics-calibrated geometry. This forces the WSI encoder to learn histopathology correlations that are predictive of the underlying genomics pattern as defined by the omics.

Since the features from both branch,  $F_{\text{N-wsi}}$  and  $F_{\text{N-omics}}$  have been normalized:  $\|F_{\text{N-wsi}}\|_2 = \|F_{\text{N-omics}}\|_2 = 1$ , the alignment process can be seen as in a spherical space and the inner product between both modalities with memory, for example,  $F_{\text{N-wsi}}^T C^+$  is equivalent to the cosine of the angle between vectors. Based on this, we introduced a soft angle-based loss for the alignment  $L_{\text{align}}$ . Let  $\phi(F, C)$  aggregate similarities over the entire memory for any  $F \in \{F_{\text{N-wsi}}, F_{\text{N-omics}}\}$ :

$$\begin{aligned} \phi(F, C) &= \frac{1}{\tau_{\text{agg}}} \ln \sum_{j=1}^n \exp(\tau_{\text{agg}} F^T c_j) \\ \phi(F, C) &\in \left[ -1 + \frac{\ln n}{\tau_{\text{agg}}}, 1 + \frac{\ln n}{\tau_{\text{agg}}} \right] \end{aligned} \quad (4)$$

with the temperature  $\tau_{\text{agg}} = 5$ , the LogSumExp function here smoothly approximates the max similarity while en-

Table 1. Internal comparison on the TCGA-BRCA dataset. The best performance is in bold, and the second-best performance is underlined.

Methods	HER2(%)			PR(%)			ODX(%)		
	AUC	ACC	F1	AUC	ACC	F1	AUC	ACC	F1
ABMIL [18]	72.9±3.1	77.1±1.8	64.8±2.9	84.5±2.3	78.8±1.6	75.0±2.1	79.3±2.5	83.8±2.6	68.8±1.6
DSMIL [20]	71.3±4.3	76.2±2.8	<u>63.5±4.1</u>	81.6±2.8	76.4±2.0	72.7±2.2	78.7±2.0	83.9±1.9	70.8±1.4
TransMIL [27]	69.8±2.8	75.6±1.9	61.1±5.2	85.2±1.0	79.0±1.2	76.1±1.6	77.9±3.5	83.5±3.7	66.8±5.0
DTFDMIL [37]	74.4±1.9	76.2±1.0	61.7±5.4	83.9±2.4	79.6±3.1	<u>76.3±2.9</u>	79.1±2.1	82.2±3.1	68.9±2.0
WIKG [21]	75.5±5.0	77.1±3.1	53.7±4.4	84.9±3.0	79.2±3.3	76.1±4.1	78.3±3.7	<u>84.1±1.2</u>	<u>71.1±2.5</u>
TDC [34]	76.2±2.1	76.7±3.9	63.3±1.1	84.7±5.3	73.1±2.1	72.3±3.1	<u>81.0±2.2</u>	81.6±3.3	70.9±2.4
MKD [38]	<u>77.1±2.3</u>	<u>77.2±5.3</u>	59.9±1.2	<u>85.1±1.2</u>	<u>80.1±1.1</u>	76.2±2.3	80.1±1.5	80.0±4.2	70.8±3.9
G-HANET [31]	76.1±5.6	71.2±6.8	62.4±4.0	85.0±2.3	79.1±3.1	75.9±5.3	80.5±1.3	81.5±4.2	71.0±5.9
<b>MoMKD</b>	<b>79.6±0.7</b>	<b>77.9±4.5</b>	<b>67.8±3.3</b>	<b>87.9±0.9</b>	<b>81.0±2.3</b>	<b>78.8±1.9</b>	<b>82.3±2.3</b>	<b>85.6±0.8</b>	<b>74.9±1.9</b>

ableng the gradient flow within all memory. We then define the memory differential as:

$$\Delta(F; C^+, C^-) = \phi(F, C^+) - \phi(F, C^-) \in [-2, 2] \quad (5)$$

For a label  $y \in \{0, 1\}$ , the  $L_{\text{align}}$  for any  $F \in \{F_{\text{N-wsi}}, F_{\text{N-omics}}\}$  is:

$$L_{\text{align}}(F, y) = \begin{cases} \text{softplus}(\beta(\text{margin} - \Delta(F; C^+, C^-))), & \text{if } y = 1 \\ \text{softplus}(\beta(\text{margin} + \Delta(F; C^+, C^-))), & \text{if } y = 0 \end{cases} \quad (6)$$

with  $\beta = 20$  as an amplifier factor, and  $\text{margin} = 0.3$  as a lower-bound of the angle differential between  $F$  and  $C$ . By enforcing this minimum tolerance, we avoid the ill posed objective of forcing perfect alignment, which could lead to overfitting. The small-batch-stable function pulls  $F$  toward the correct memory  $C$  while pushing it away from the other memory, encoding the class boundary directly in memory geometry without relying on large contrastive batches. Throughout the training progress, the memory receives information from both modalities and serves as a semantic bottleneck, forcing the WSI encoder to filter out intra-batch noise and retain only the core semantics relevant to the omics modality.

**Memory Evolution via Gradient Decoupling.** A core challenge is the fundamental asymmetry between modalities: omics data is often a dominant predictor for biomarkers, while WSI features are high-dimensional and sparse. The direct joint-training approach would allow the powerful omics gradient to overwhelm the WSI branch. We therefore decouple the branches: there is no direct gradient flow between WSI and omics. Their only interaction is indirect, mediated exclusively by the memory via the alignment loss. Furthermore, we must shield the memory itself from the strong, task-specific gradients of the classification head. Allowing the classifier’s loss to backpropagate into

the memory would cause memory collapse, as this dominant signal would corrupt the memory being accumulated. In short, the memory evolution is governed by (i) the  $L_{\text{mem}}$  which regularizes and maintains orthogonality (introduced in Section 3.5); (ii) the  $L_{\text{align}}$  keeps the memory shaped by meaningful cross-modal alignment; (iii) the reconstruction loss  $L_{\text{mse}}$  maintain its internal genomics structure.

### 3.4. Memory-guided Uni-modal Inference

During uni-modal inference, the accumulated memory is retrieved. Each patch-level projection  $F_{P\text{-wsi},i}$  is evaluated by its differential affinity to memory representations:

$$\text{Score}_i = \max_j (F_{P\text{-wsi},i}^\top c_j^+) - \max_j (F_{P\text{-wsi},i}^\top c_j^-), \quad (7)$$

This difference reflects how strongly each patch aligns with the omics-positive visual concept. The resulting attention weights are computed with a temperature  $\tau = 0.2$ :

$$\alpha_i = \frac{e^{\text{Score}_i/\tau}}{\sum_j e^{\text{Score}_j/\tau}} \quad (8)$$

so that patches more consistent with genomics informative patterns receive higher attention. The final slide-level representation is obtained as a weighted aggregation:

$$F_{C\text{-wsi}} = \sum_{i=1}^I \alpha_i F_{\text{wsi},i} \in \mathbb{R}^D, D = 128 \quad (9)$$

which is subsequently passed through the final linear layer  $g(\cdot)$  to generate the slide-level prediction  $g(F_{C\text{-wsi}})$ . According to this, the momentum memory acts as a set of global genomics anchors that guide the attention mechanism, providing robust predictions.

### 3.5. Training Objective

The final objective combines cross-entropy loss  $L_{\text{ce}}$ , reconstruction loss  $L_{\text{mse}}$ , cross-modal alignment  $L_{\text{align}}$ , and mem-

Table 2. External validation results for the ODX prediction task on the independent in-house dataset. The best performance is in bold, and the second-best performance is underlined.

Methods	In-house dataset(%)		
	AUC	ACC	F1
ABMIL	75.1±1.7	86.1±0.2	60.9±3.7
DSMIL	74.3±2.8	86.1±0.7	61.2±3.2
TransMIL	71.7±2.4	85.0±1.7	60.5±4.1
DTFDMIL	76.2±2.2	<u>86.5±1.5</u>	<u>63.5±3.9</u>
WIKG	75.9±3.5	86.7±1.4	58.3±5.3
TDC	<u>76.5±2.1</u>	86.2±3.0	<u>63.5±3.2</u>
MKD	76.2±2.0	86.1±2.9	61.0±6.3
G-HANET	76.1±1.3	86.4±2.2	63.1±6.4
<b>MoMKD</b>	<b>79.4±0.8</b>	<b>87.1±1.7</b>	<b>68.0±3.0</b>

ory regularization  $L_{\text{mem}}$ :

$$\begin{aligned}
 L_{\text{total}} = & \lambda_{\text{ce}} L_{\text{ce}}(g(F_{\text{C-wsi}}), y) \\
 & + \lambda_{\text{mse}} L_{\text{mse}}(\text{omics}, \text{Decoder}(F_{\text{omics}})) \\
 & + \alpha_{\text{wsi}} L_{\text{align}}(F_{\text{N-wsi}}, y) + \alpha_{\text{omics}} L_{\text{align}}(F_{\text{N-omics}}, y) \\
 & + \lambda_{\text{mem}} L_{\text{mem}}
 \end{aligned} \tag{10}$$

Here,  $L_{\text{mem}}$  is defined as:

$$\begin{aligned}
 L_{\text{mem}} = & \frac{1}{I} \sum_{i=1}^I \|F_{\text{N-wsi},i} - \text{sg}(c_{k_i^*})\|_2^2 \\
 & + \sum_{i=1}^n \sum_{j \neq i}^n \left( \frac{c_i^\top c_j}{\|c_i\|_2 \|c_j\|_2} \right)^2
 \end{aligned} \tag{11}$$

where  $k_i^* = \arg \min_j \|F_{\text{N-wsi},i} - c_j\|_2$  denotes the index of the memory closest to the  $i$ -th patch feature, and  $c_{k_i^*}$  represents the corresponding centroid retrieved from the memory bank. The operator  $\text{sg}(\cdot)$  indicates the stop-gradient function, which treats its argument as a constant during back-propagation to prevent the memory bank from being updated via direct gradient flow. For the hyperparameters in  $L_{\text{total}}$ , we apply  $\lambda_{\text{ce}} = 0.5$ ,  $\lambda_{\text{mse}} = 0.01$ ,  $\alpha_{\text{omics}} = 0.05$ ,  $\alpha_{\text{wsi}} = 0.2$ , and  $\lambda_{\text{mem}} = 0.1$ .

## 4. Experiments and Results

### 4.1. Experimental Setup

**Datasets.** To demonstrate the effectiveness of the proposed QKD method, we conduct extensive experiments on three different tasks based on the TCGA-BRCA dataset [32] for HER2, PR, Oncotype-DX (ODX) score classification. This dataset contains a multi-omics resource. For each task, we build the cohort based on labels provided in the official

Table 3. Ablation study on the proposed method. **OMICS\*** indicates the inclusion of the omics reconstruction task.

Modality		Aligning objective			AUC (%)
WSI	OMICS	WSI	OMICS	OMICS*	
✓	—	—	—	—	73.9±3.1
✓	✓	✓	—	✓	74.2±3.6
✓	✓	—	—	✓	75.7±2.5
✓	✓	✓	✓	—	78.0±3.6
✓	✓	✓	—	✓	75.1±4.0
✓	✓	✓	—	✓	<b>79.6±0.7</b>

documentation; the overall label distribution: HER2: 141 (positive): 668 (negative), PR: 649 (positive): 351 (negative), ODX: 282 (positive): 715 (negative). To evaluate the generalizability of the method, we collected an in-house dataset which provides 1127 breast cancer pathology slides with an ODX score distribution of 162 (positive): 961 (negative). More information for each dataset can be found in supplementary materials.

**Implementation Details.** For the TCGA-BRCA dataset, we performed patient-level five-fold stratified splitting with the ratio of 7:1:2 for each task and reported the average test metrics across five folds. The in-house dataset serves as the external validation set for the ODX task, which is tested by five models trained on the TCGA-BRCA dataset with the average results reported. More details and code are available in the supplementary material. For the evaluation, we collected five WSI-only MIL approaches (ABMIL [18], DSMIL [20], TransMIL [27], DTFDMIL [37], WIKG [21]) and three multimodal knowledge distillation methods (TDC [34], MKD [38], G-HANet [31]) for the comprehensive comparison.

### 4.2. Experimental Results

**Internal Comparison.** Table 1 shows the results of different classification tasks (HER2, PR, and ODX) on the TCGA-BRCA dataset. As shown in the table, our method consistently outperformed alternative models across all three tasks. Compared with the best-performing WSI-only MIL model (WIKG), our method achieved AUC improvements of +7.0%, +3.5%, and +5.1% on the HER2, PR, and ODX tasks, respectively. Compared to the SOTA multimodal KD baseline (MKD), our method still yielded notable gains, achieving AUCs of 79.6%, 87.9%, and 82.3% for the three tasks. These results highlight the effectiveness of the momentum memory distillation design, which enables more discriminative feature alignment between pathology and transcriptomic modalities, thereby improving performance across genomics-sensitive prediction tasks.

Table 4. Fixed memory vs. momentum memory.

Task	AUC (%)	
	Fixed	Momentum
HER2	75.2±3.0	<b>79.6±0.7</b>
PR	84.7±2.1	<b>87.9±0.9</b>
ODX	81.9±2.3	<b>82.3±2.3</b>
In-house dataset	73.5±3.7	<b>79.4±0.8</b>

**External Comparison.** To further assess the generalizability of the proposed MoMKD framework, we conducted experiments on the in-house dataset for the ODX prediction task. As summarized in Table 2, our method consistently outperformed all competing approaches. Specifically, our method achieved the highest AUC of 79.4%, accuracy of 87.1%, and F1-score of 68.0%, surpassing the best multi-modal competitor (TDC, AUC = 76.5%) by 3.8% in AUC and 7.1% in F1-score. These results confirmed that the accumulated memory alignment enhances cross-domain stability, supporting our hypothesis that momentum-updated memory provides robust data representation for the distribution shift problem.

### 4.3. Ablation Study

**Effects on each component** To evaluate the distillation performance within the proposed MoMKD framework, we conducted a series of ablation experiments based on the HER2 task, as summarized in Table 3. The WSI-only baseline model achieved an AUC of  $73.9 \pm 3.1\%$ . First, to isolate the memory’s effect as a visual regularizer, we set  $\alpha_{\text{omics}} = 0$ , forcing the memory to be shaped only by WSI features; this configuration alone improved performance to  $75.2 \pm 2.4\%$ , which indicates the momentum memory can increase the learning capacity of the model. Conversely, incorporating the omics alignment objective alone ( $\alpha_{\text{wsi}} = 0$ ), in other words, the omics data actively shapes the geometry of the memory, but the WSI branch only “sees” this genetic-calibrated memory for the final aggregation. This resulted in an AUC of  $75.7 \pm 2.5\%$ , strongly indicating that the primary performance gain stems from aligning with a stable, genomics-defined memory rather than simple visual consistency. Furthermore, the importance of a stable omics prior was confirmed, as removing the omics self-reconstruction task degraded performance to  $78.0 \pm 3.6\%$ . Finally, the complete MoMKD framework, optimizing both WSI and omics alignment objectives jointly, achieved the highest performance of  $79.6 \pm 0.7\%$ , demonstrating the synergistic effect of all components.

**Fixed memory bank v.s. momentum memory** To isolate the critical contribution of our dynamic memory up-

date, we compared MoMKD against a fixed memory bank baseline. This baseline uses the exact same K-means initialization, but the memory is subsequently frozen throughout training, reducing it to a static dictionary. As shown in Table 4, our momentum-driven approach yields superior performance across all tasks, including significant gains on HER2 (+4.5%) and the in-house ODX dataset (+5.9%). The crucial limitation of the fixed approach is revealed under domain shift. While the fixed setting achieved a high AUC ( $81.1 \pm 2.7\%$ ) on the public ODX cohort, its performance collapsed to  $73.5 \pm 3.7\%$  on the in-house data, indicating severe overfitting to the source domain’s initial visual representation. In contrast, MoMKD, with its momentum memory, maintained strong cross-cohort robustness ( $79.4 \pm 0.8\%$ ). This provides clear evidence that the momentum update is essential: it transforms the memory from a static target into a dynamic semantic center. By continuously tracking the global data distribution and smoothing batch-level noise, our method builds a robust semantic representation that generalizes effectively.

**Momentum memory update across tasks.** Figure 3 summarizes the training dynamics of the memory storage across three prediction tasks. In all cases, the active memory ratio remains above 0.75, indicating that most memory components participate in the training trajectory. The perplexity profiles show task-specific differences: As the most difficult task, HER2 statues majorly be identified by IHC stain instead of H&E stain [1, 26], it maintains a larger number of active memory components to represent the sparse signal, while PR and ODX converge to lower values since the model can identify more visual signals from the image [11]. These observations highlight that momentum memory adapts its effective capacity to task complexity, achieving both stability and compactness. Detailed definitions of these metrics and additional analyses within the in-house dataset are provided in Supplementary Material Section S3.

**Effects on the memory size** Figure S1 in the supplementary material presents the variation of memory size in different tasks, and the MoMKD framework performs consistently.

### 4.4. Visualization and Interpretation

To interpret the memory behavior, we visualized the spatial distribution of memory activations on WSIs and examined the corresponding patch-level patterns under the guidance of experienced pathologists. Here we randomly collect four memory components in each memory set with the top three corresponding patches based on the ODX task, as shown in Figure 4.

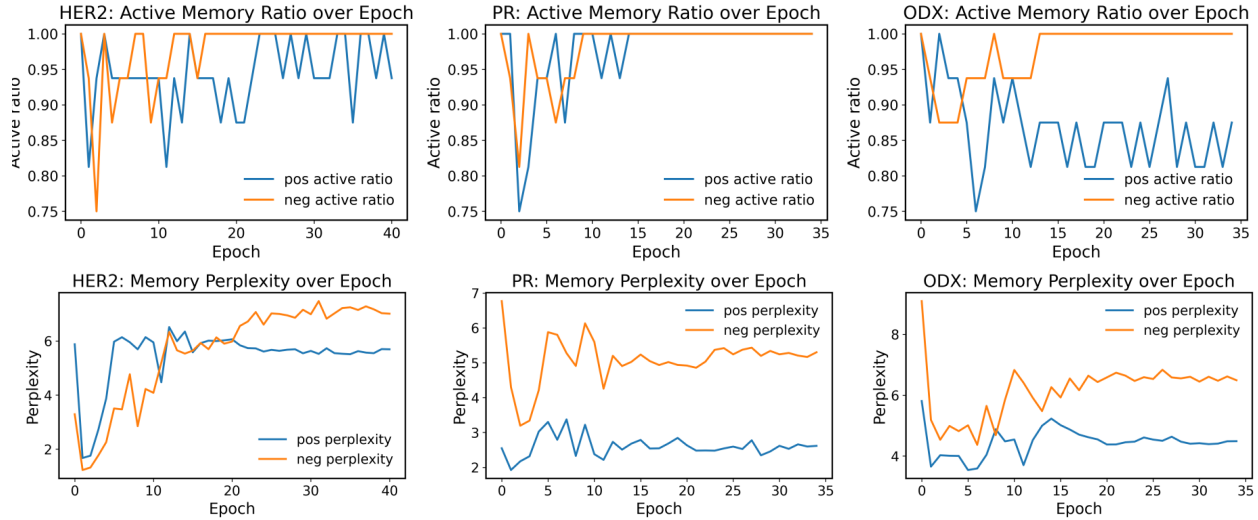


Figure 3. **Memory dynamics across biomarker prediction tasks.** Each column corresponds to one task (**HER2**, **PR**, and **ODX**), while each row depicts one statistic of the memory storage: (**upper**) *Active memory Ratio*, and (**bottom**) *Perplexity*. The active memory ratio quantifies the proportion of memory components utilized during training, ensuring that no dead memory components emerge. The corresponding perplexity represents the effective number of active memory components ( $c_j^+$  and  $c_j^-$ ). Across all tasks, the momentum memory maintains high active ratios ( $> 0.75$ ) and perplexity, indicating stable and interpretable utilization of the memory storage.

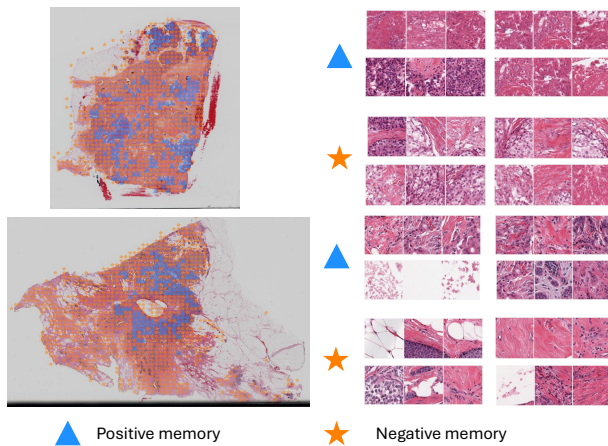


Figure 4. The visualization result based on memory with the mapped patches in WSI. The upper figure is the positive case with the lower one is negative based on Oncotype DX test. For each memory component, we present the top-3 mapped patches here.

Under expert pathological review, it showed the top-ranked image patches (right panel) demonstrate that the positive memory are predominantly activated within tumor-rich and stromal interaction regions, capturing dense epithelial clusters, nuclear pleomorphism, and desmoplastic stroma, which are histopathology consistent with aggressive tumor behavior. In contrast, negative memory respond primarily to benign-appearing structures such as adipose tissue, normal ducts, and fibrous stroma. The top-ranked

image patches further confirm that each memory part consistently encodes an interpretable histologic pattern. These findings validate that the learned memory indeed capture biologically meaningful features.

## 5. Discussion

Overall, our findings demonstrate that the momentum memory plays a central role in stabilizing cross-modal distillation between histopathology and genomics. The memory maintains highly semantic diversity, avoids global collapse, and adapts its usage patterns to the morphological complexity of each biomarker prediction task. Comparisons with static memory further highlight that dynamic, momentum-driven updates are essential for resisting domain shift and constructing a robust semantic representation. These observations suggest that momentum memory is not merely a storage mechanism, but a dynamic semantic aggregator that balances expressivity and compactness. This provides a principled foundation for future multimodal distillation frameworks and opens new possibilities for interpretable and generalizable computational pathology models.

## 6. Conclusion

The cross-modal distillation between histopathology and genomics is hindered by fragile, batch-local alignments. This work presents MoMKD, a Momentum Memory for Knowledge Distillation framework that reframes this problem as alignment to a stable and class-conditioned momentum memory. Across multiple biomarker prediction

tasks (HER2, PR, ODX) on TCGA-BRCA and an independent in-house validation cohort, the proposed method consistently outperforms both WSI-only and multimodal baselines, demonstrating strong generalization and robustness under domain shift. It further indicates that the proposed method successfully bridges the asymmetry between genomics and histopathology modalities. In summary, MoMKD introduces a cross-batch multimodal paradigm for computational pathology, establishing a generalizable principle for stable and interpretable knowledge distillation.

## References

- [1] HER2 Testing in Breast Cancer - 2023 Guideline Update. <https://www.cap.org/protocols-and-guidelines/cap-guidelines/current-cap-guidelines/recommendations-for-human-epidermal-growth-factor-2-testing-in-breast-cancer>. 7
- [2] David Ahmedt-Aristizabal, Mohammad Ali Armin, Simon Denman, Clinton Fookes, and Lars Petersson. A survey on graph-based deep learning for computational histopathology. *Computerized Medical Imaging and Graphics*, 95:102027, 2022. 2
- [3] Alev Baysoy, Zhiliang Bai, Rahul Satija, and Rong Fan. The technological landscape and applications of single-cell multi-omics. *Nature Reviews. Molecular Cell Biology*, pages 1–19, 2023. 1
- [4] Qi Bi, Xu Sun, Shuang Yu, Kai Ma, Cheng Bian, Munan Ning, Nanjun He, Yawen Huang, Yuexiang Li, Hanruo Liu, and Yefeng Zheng. MIL-ViT: A multiple instance vision transformer for fundus image classification. *Journal of Visual Communication and Image Representation*, 97:103956, 2023. 2
- [5] Gianpaolo Bontempo, Federico Bolelli, Angelo Porrello, Simone Calderara, and Elisa Ficarra. A Graph-Based Multi-Scale Approach With Knowledge Distillation for WSI Classification. *IEEE Transactions on Medical Imaging*, 43(4):1412–1421, 2024. 2
- [6] Shaked Brody, Uri Alon, and Eran Yahav. How Attentive are Graph Attention Networks?, 2022. 4
- [7] Cheng Chen, Qi Dou, Yueming Jin, Quande Liu, and Pheng Ann Heng. Learning With Privileged Multimodal Knowledge for Unimodal Segmentation. *IEEE Transactions on Medical Imaging*, 41(3):621–632, 2022. 2
- [8] Richard J Chen, Ming Y Lu, Wei-Hung Weng, Tiffany Y Chen, Drew FK Williamson, Trevor Manz, Maha Shady, and Faisal Mahmood. Multimodal co-attention transformer for survival prediction in gigapixel whole slide images. In *Proceedings of the IEEE/CVF international conference on computer vision*, pages 4015–4025, 2021. 1
- [9] Richard J Chen, Ming Y Lu, Drew FK Williamson, Tiffany Y Chen, Jana Lipkova, Zahra Noor, Muhammad Shaban, Maha Shady, Mane Williams, Bumjin Joo, et al. Pan-cancer integrative histology-genomic analysis via multimodal deep learning. *Cancer cell*, 40(8):865–878, 2022. 1
- [10] Ting Chen, Simon Kornblith, Mohammad Norouzi, and Geoffrey Hinton. A Simple Framework for Contrastive Learning of Visual Representations. In *Proceedings of the 37th International Conference on Machine Learning*, pages 1597–1607. PMLR, 2020. 3
- [11] Melina B. Flanagan, David J. Dabbs, Adam M. Brufsky, Sushil Beriwal, and Rohit Bhargava. Histopathologic variables predict Oncotype DX™ Recurrence Score. *Modern Pathology*, 21(10):1255–1261, 2008. 7
- [12] Rushin H. Gindra, Giovanni Palla, Mathias Nguyen, Sophia J. Wagner, Manuel Tran, Fabian J. Theis, Dieter Saur, Lorin Crawford, and Tingying Peng. A Large-Scale Benchmark of Cross-Modal Learning for Histology and Gene Expression in Spatial Transcriptomics. In *Proceedings of the IEEE/CVF International Conference on Computer Vision*, pages 1182–1192, 2025. 2
- [13] Yongxin Guo, Ziyu Su, Onur C. Koyun, Hao Lu, Robert Wesolowski, Gary Tozbikian, M. Khalid Khan Niazi, and Metin N. Gurcan. BPMambaMIL: A bio-inspired prototype-guided multiple instance learning for oncotype DX risk assessment in histopathology. *Computer Methods and Programs in Biomedicine*, 272:109039, 2025. 1
- [14] Metin N. Gurcan, Laura E. Boucheron, Ali Can, Anant Madabhushi, Nasir M. Rajpoot, and B. Yener. Histopathological image analysis: A review. *IEEE reviews in biomedical engineering*, 2:147–171, 2009. 1
- [15] Jiabang He, Jia Liu, Lei Wang, Xiyao Li, and Xing Xu. Mo-CoSA: Momentum Contrast for Knowledge Graph Completion with Structure-Augmented Pre-trained Language Models. In *2024 IEEE International Conference on Multimedia and Expo (ICME)*, pages 1–6, 2024. 3
- [16] Kaiming He, Haoqi Fan, Yuxin Wu, Saining Xie, and Ross Girshick. Momentum Contrast for Unsupervised Visual Representation Learning, 2020. 2, 3
- [17] Geoffrey Hinton, Oriol Vinyals, and Jeff Dean. Distilling the Knowledge in a Neural Network, 2015. 2
- [18] Maximilian Ilse, Jakub Tomczak, and Max Welling. Attention-based Deep Multiple Instance Learning. In *Proceedings of the 35th International Conference on Machine Learning*, pages 2127–2136. PMLR, 2018. 2, 5, 6
- [19] Sajid Javed, Arif Mahmood, Talha Kaiser, and Naoufel Werghi. Knowledge Distillation in Histology Landscape by Multi-Layer Features Supervision. *IEEE Journal of Biomedical and Health Informatics*, 27(4):2037–2046, 2023. 2
- [20] Bin Li, Yin Li, and Kevin W. Eliceiri. Dual-stream multiple instance learning network for whole slide image classification with self-supervised contrastive learning. In *Proceedings of the IEEE/CVF Conference on Computer Vision and Pattern Recognition*, pages 14318–14328, 2021. 5, 6
- [21] Jiawen Li, Yuxuan Chen, Hongbo Chu, Qiehe Sun, Tian Guan, Anjia Han, and Yonghong He. Dynamic Graph Representation with Knowledge-Aware Attention for Histopathology Whole Slide Image Analysis. In *2024 IEEE/CVF Conference on Computer Vision and Pattern Recognition (CVPR)*, pages 11323–11332, Seattle, WA, USA, 2024. IEEE. 2, 5, 6
- [22] Ming Y. Lu, Drew F. K. Williamson, Tiffany Y. Chen, Richard J. Chen, Matteo Barbieri, and Faisal Mahmood. Data-efficient and weakly supervised computational pathol-

- ogy on whole-slide images. *Nature Biomedical Engineering*, 5(6):555–570, 2021. 2
- [23] Jiabo Ma, Zhengrui Guo, Fengtao Zhou, Yihui Wang, Yingxue Xu, Jinbang Li, Fang Yan, Yu Cai, Zhengjie Zhu, Cheng Jin, Yi Lin, Xinrui Jiang, Chenglong Zhao, Danyi Li, Anjia Han, Zhenhui Li, Ronald Cheong Kin Chan, Jiguang Wang, Peng Fei, Kwang-Ting Cheng, Shaoting Zhang, Li Liang, and Hao Chen. A generalizable pathology foundation model using a unified knowledge distillation pretraining framework. *Nature Biomedical Engineering*, pages 1–20, 2025. 2
- [24] Rajeev Nema. An omics-based tumor microenvironment approach and its prospects. *Reports of Practical Oncology and Radiotherapy*, 29(5):649–650, 2024. 1
- [25] Muhammad Khalid Khan Niazi, Anil V. Parwani, and Metin N. Gurcan. Digital pathology and artificial intelligence. *The lancet oncology*, 20(5):e253–e261, 2019. 1
- [26] Gil Shamaï, Ran Schley, Alexandra Cretu, Tal Neoran, Edmond Sabo, Yoav Binenbaum, Shachar Cohen, Tal Goldman, António Polónia, Keren Drumea, Karin Stoliar, and Ron Kimmel. Clinical utility of receptor status prediction in breast cancer and misdiagnosis identification using deep learning on hematoxylin and eosin-stained slides. *Communications Medicine*, 4(1):276, 2024. 7
- [27] Zhuchen Shao, Hao Bian, Yang Chen, Yifeng Wang, Jian Zhang, Xiangyang Ji, and yongbing zhang. TransMIL: Transformer based Correlated Multiple Instance Learning for Whole Slide Image Classification. In *Advances in Neural Information Processing Systems*, pages 2136–2147. Curran Associates, Inc., 2021. 2, 5, 6
- [28] Tong Shu, Jun Shi, Dongdong Sun, Zhiguo Jiang, and Yushan Zheng. SlideGCD: Slide-Based Graph Collaborative Training with Knowledge Distillation for Whole Slide Image Classification. In *Medical Image Computing and Computer Assisted Intervention – MICCAI 2024*, pages 470–480, Cham, 2024. Springer Nature Switzerland. 2
- [29] Ziyu Su, Yongxin Guo, Robert Wesolowski, Gary Tozbikian, Nathaniel S. O’Connell, M. Khalid Khan Niazi, and Metin N. Gurcan. Computational Pathology for Accurate Prediction of Breast Cancer Recurrence: Development and Validation of a Deep Learning-based Tool, 2024. 1
- [30] Kang Wang, Feiyang Zheng, Dayan Guan, Jia Liu, and Jing Qin. Distilling heterogeneous knowledge with aligned biological entities for histological image classification. *Pattern Recognition*, 160:111173, 2025. 2
- [31] Zhikang Wang, Yumeng Zhang, Yingxue Xu, Seiya Imoto, Hao Chen, and Jiangning Song. Histo-Genomic Knowledge Distillation For Cancer Prognosis From Histopathology Whole Slide Images, 2024. 2, 5, 6
- [32] John N. Weinstein, Eric A. Collisson, Gordon B. Mills, Kenna R. Mills Shaw, Brad A. Ozenberger, Kyle Ellrott, Ilya Shmulevich, Chris Sander, and Joshua M. Stuart. The Cancer Genome Atlas Pan-Cancer analysis project. *Nature Genetics*, 45(10):1113–1120, 2013. 6
- [33] Zhirong Wu, Yuanjun Xiong, Stella X. Yu, and Dahua Lin. Unsupervised Feature Learning via Non-Parametric Instance Discrimination. In *Proceedings of the IEEE Conference on Computer Vision and Pattern Recognition*, pages 3733–3742, 2018. 3
- [34] Xiaohan Xing, Meilu Zhu, Zhen Chen, and Yixuan Yuan. Comprehensive learning and adaptive teaching: Distilling multi-modal knowledge for pathological glioma grading. *Medical Image Analysis*, 91:102990, 2024. 2, 5, 6
- [35] Yingxue Xu and Hao Chen. Multimodal optimal transport-based co-attention transformer with global structure consistency for survival prediction. In *Proceedings of the IEEE/CVF International Conference on Computer Vision (ICCV)*, pages 21241–21251, 2023. 1
- [36] Yunfang Yu, Gengyi Cai, Ruichong Lin, Zehua Wang, Yongjian Chen, Yujie Tan, Zifan He, Zhuo Sun, Wenhao Ouyang, Herui Yao, and Kang Zhang. Multimodal data fusion AI model uncovers tumor microenvironment immunotyping heterogeneity and enhanced risk stratification of breast cancer. *MedComm*, 5(12):e70023, 2024. 1
- [37] Hongrun Zhang, Yanda Meng, Yitian Zhao, Yihong Qiao, Xiaoyun Yang, Sarah E. Coupland, and Yalin Zheng. DTFD-MIL: Double-Tier Feature Distillation Multiple Instance Learning for Histopathology Whole Slide Image Classification, 2022. 5, 6
- [38] Qibin Zhang, Xinyu Hao, Qiao Chen, Rui Xu, Fengyu Cong, Cheng Lu, and Hongming Xu. Multi-modal Knowledge Decomposition based Online Distillation for Biomarker Prediction in Breast Cancer Histopathology, 2025. 2, 5, 6
- [39] Yan Zhang, Zhong Ji, Di Wang, Yanwei Pang, and Xuelong Li. USER: Unified Semantic Enhancement With Momentum Contrast for Image-Text Retrieval. *IEEE Transactions on Image Processing*, 33:595–609, 2024. 3
- [40] Yupei Zhang, Xiaofei Wang, Anran Liu, Lequan Yu, and Chao Li. Disentangled Multi-modal Learning of Histology and Transcriptomics for Cancer Characterization, 2025. 2
- [41] Wenhui Zhu, Xiwen Chen, Peijie Qiu, Aristeidis Sotiras, Abolfazl Razi, and Yalin Wang. DGR-MIL: Exploring Diverse Global Representation in Multiple Instance Learning for Whole Slide Image Classification. In *Computer Vision – ECCV 2024*, pages 333–351, Cham, 2025. Springer Nature Switzerland. 1
- [42] Wenxuan Zou, Xingqun Qi, Zhuojie Wu, Zijian Wang, Muyi Sun, and Caifeng Shan. CoCo DistillNet: A Cross-layer Correlation Distillation Network for Pathological Gastric Cancer Segmentation. In *2021 IEEE International Conference on Bioinformatics and Biomedicine (BIBM)*, pages 1227–1234, 2021. 2